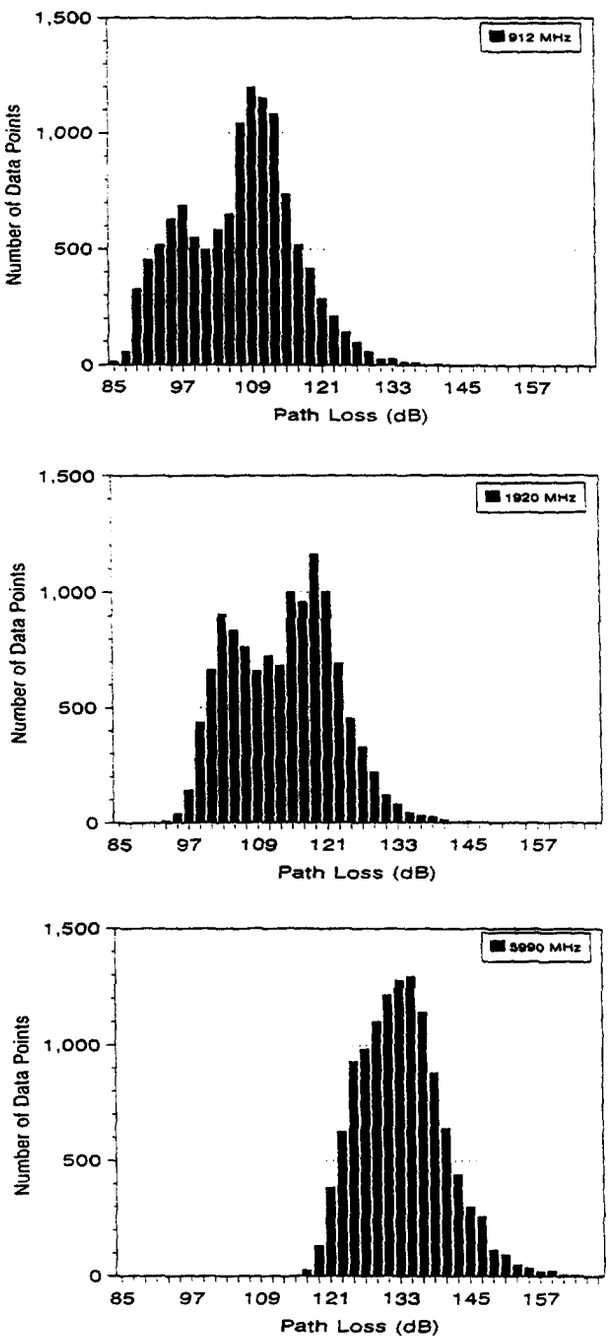

Figure C-26. Path loss distribution for high rise 4, floor 15, NLOS.

APPENDIX D: BUILDING PENETRATION LOSS DATA

The following tables show the calculated penetration losses for the residential and high-rise buildings measured.

Table D-1. Mean LOS Penetration Losses for Each Residence

Frequency (MHz)	Residence	Mean Loss (dB)	σ (dB)
912	1	6.3	6.3
	2	4.9	6.6
	3	8.1	7.1
	4	4.6	6.6
	5	9.2	7.4
	6	9.0	7.2
	7	9.1	7.6
1920	1	7.0	7.4
	2	8.3	7.5
	3	12.4	8.9
	4	6.7	7.9
	5	11.1	9.8
	6	9.9	10.2
	7	12.5	8.7
5990	1	10.7	7.7
	2	9.3	7.1
	3	18.5	10.3
	4	14.1	9.1
	5	16.6	10.4
	6	13.2	10.8
	7	17.9	9.9

Table D-2. Mean NLOS Penetration Losses for Each Residence

Frequency (MHz)	Residence	Mean Loss (dB)	σ (dB)
912	1	6.1	6.1
	2	2.9	6.0
	3	5.8	6.6
	4	6.4	6.2
	5	10.5	7.6
	6	7.3	7.3
	7	6.5	6.3
1920	1	8.4	6.9
	2	3.6	8.0
	3	12.3	8.6
	4	9.8	6.4
	5	11.8	10.5
	6	8.9	8.7
	7	11.6	7.5
5990	1	10.2	7.4
	2	11.5	9.0
	3	18.5	9.4
	4	12.5	7.5
	5	11.8	11.0
	6	13.4	9.3
	7	13.6	8.5

Table D-3. Mean Penetration Losses for All Residences (Calculated From Tables D-1 and D-2)

Path	Frequency (MHz)	Mean Loss (dB)
LOS	912	6.9
NLOS		6.0
Both		6.4
LOS	1920	8.3
NLOS		8.4
Both		8.4
LOS	5990	11.1
NLOS		12.5
Both		11.7

Table D-4. Mean LOS Penetration Losses per Floor for Each Residence

Residence	Frequency (MHz)	Mean Loss (dB)		
		Ground Floor	Second Floor	Basement
1	912 1920 5990	5.7 6.0 9.5	N/A	12.9 17.8 21.8
2	912 1920 5990	3.8 6.7 7.8	7.2 13.4 13.7	N/A
3	912 1920 5990	7.1 11.2 17.3	N/A	15.3 27.5 36.7
4	912 1920 5990	5.5 6.7 16.2	N/A	N/A
5	912 1920 5990	8.1 10.9 17.6	9.2 9.5 14.0	19.9 30.6 38.8
6	912 1920 5990	7.2 7.8 12.8	9.5 10.5 11.7	18.1 29.1 35.3
7	912 1920 5990	7.8 11.1 17.2	8.6 10.1 16.7	19.6 26.2 37.5
Mean	912 1920 5990	6.5 8.6 14.1	8.6 10.9 14.0	15.2 26.2 34.0

Table D-5. Mean Penetration Losses for Each High Rise

Path	Frequency (MHz)	High Rise	Mean Loss (dB)	σ (dB)
LOS	912	1	14.2	8.8
		2	11.2	9.4
		3	14.4	12.5
		4	7.4	12.1
	1920	1	11.6	9.6
		2	15.4	11.1
		3	16.6	14.5
		4	10.0	14.3
	5990	1	17.6	9.4
		2	19.4	11.0
		3	23.2	14.5
		4	19.0	13.0
NLOS	912	1	14.0	7.5
		2	11.7	6.3
		3	13.9	9.5
		4	8.0	10.7
	1920	1	12.4	8.2
		2	14.8	7.7
		3	20.1	10.9
		4	5.9	10.8
	5990	1	20.9	7.2
		2	19.2	7.0
		3	25.5	9.3
		4	16.4	8.8

Table D-6. Mean Penetration Losses for All High-rise Buildings (Calculated From Table D-4)

Path	Frequency (MHz)	Mean Loss (dB)
LOS	912	11.1
NLOS		11.2
Both		11.2
LOS	1920	13.9
NLOS		10.5
Both		11.9
LOS	5990	20.7
NLOS		19.4
Both		20.0

FORM **NTIA-29**
(4-80)

U.S. DEPARTMENT OF COMMERCE
NAT'L. TELECOMMUNICATIONS AND INFORMATION ADMINISTRATION

BIBLIOGRAPHIC DATA SHEET

	1. PUBLICATION NO.	2. Gov't Accession No.	3. Recipient's Accession No.
	95-325		

4. TITLE AND SUBTITLE

Building Penetration Measurements from Low-Height Base Stations at 912, 1920, and 5990 MHZ

5. Publication Date

6. Performing Organization Code
NTIA/ITS

7. AUTHOR(S)
Lynette H. Loew, Yeh Lo, Michael G. Laflin, Elizabeth E. Pol

9. Project/Task/Work Unit No.
5 910 5105

8. PERFORMING ORGANIZATION NAME AND ADDRESS

National Telecommunications and Information Administration
Institute for Telecommunication Sciences
325 Broadway
Boulder, CO 80303-3328

10. Contract/Grant No.

11. Sponsoring Organization Name and Address

12. Type of Report and Period Covered

13.

14. SUPPLEMENTARY NOTES

15. ABSTRACT *(A 200-word or less factual summary of most significant information. If document includes a significant bibliography or literature survey, mention it here.)*

Building penetration measurements were taken simultaneously at three potential Personal Communications Services (PCS) frequencies: 912, 1920, and 5990 MHz. The continuous wave (CW) measurement system employed a fixed outdoor transmitter and a mobile indoor receiver. The goal was to quantify building penetration losses at these frequencies to determine the viability of indoor coverage using street microcells and base antenna heights below the roof level of surrounding buildings. Eleven different buildings representing typical residential and high-rise office building environments were used for the measurements. Vertically polarized transmit and receive antennas were used for all measurements. Statistical analyses of the data include mean building attenuation losses, standard deviations, cumulative probability distribution functions, and correlation coefficients. The analyses were used to characterize propagation effects and provide a comparison between three frequencies, two cell environments, and two transmission paths.

16. Key Words *(Alphabetical order, separated by semicolons)*

attenuation; building attenuation; building penetration; measurements; personal communications services; PCS; penetration characteristics; penetration loss; radio propagation

17. AVAILABILITY STATEMENT

☒ UNLIMITED.

☐ FOR OFFICIAL DISTRIBUTION.

18. Security Class. *(This report)*
Unclassified

20. Number of pages
123

19. Security Class. *(This page)*
Unclassified

21. Price:

*U.S. GOVERNMENT PRINTING OFFICE:1995-673-018/00132

Biological Effects of Electromagnetic Radiation

Edited by

John M. Osepchuk

Consulting Scientist
Raytheon Research Division

Associate Editors

James W. Frazer, Ross University Medical School, Dominica, West Indies
Om P. Gandhi, Departments of Electrical Engineering and Bioengineering, University of Utah
Arthur W. Guy, School of Medicine, University of Washington
Don R. Justesen, Veterans Administration Medical Center, Kansas City
Sol M. Michaelson, School of Medicine and Dentistry, University of Rochester
John C. Mitchell, USAF School of Aerospace Medicine, Brooks Air Force Base

A volume in the IEEE PRESS Selected Reprint Series, prepared under the sponsorship of the IEEE Committee on Man and Radiation.

IEEE PRESS

The Institute of Electrical and Electronics Engineers, Inc., New York

Sole Worldwide Distributor (Exclusive of the IEEE)

JOHN WILEY & SONS, INC.
605 Third Ave.
New York, NY 10158

Wiley Order Number: 471-88787-0
IEEE Order Number: PC01594

Library of Congress Cataloging in Publication Data
Main entry under title:

Biological effects of electromagnetic radiation.

(IEEE Press selected reprint series)
Includes bibliographies and indexes.
1. Electromagnetism—Physiological effect—Addresses, essays, lectures. I. Osepchuk, John M.
QP82.2.E43B554 1983 599'.019151 82-23380
ISBN 0-87942-165-7

Nonionizing Electromagnetic Wave Effects in Biological Materials and Systems

CURTIS C. JOHNSON, SENIOR MEMBER, IEEE, AND ARTHUR W. GUY, MEMBER, IEEE

Invited Paper

***Abstract*—Electromagnetic waves from the lower radio frequencies up through the optical spectrum can generate a myriad of effects and responses in biological specimens. Some of these effects can be harmful to man at high radiation intensities, producing burns, cataracts, chemical changes, etc. Biological effects have been reported at lower radiation intensities, but it is not now known if low-level effects are harmful. Even behavioral changes have been reported. Most of the effects are not harmful under controlled conditions, and can thereby be used for therapeutic purposes and to make useful diagnostic measurements. The problem of microwave penetration into the body with resultant internal power absorption is approached from both the theoretical and the experimental viewpoints. The results are discussed in terms of therapeutic warming of tissues and possible hazards caused by internal "hot spots." The absorption and scattering effects of light in biological tissues are reviewed. Molecular absorption peaks in the optical spectrum are useful for making molecular concentration measurements by spectroscopy. Much of the related work in the literature is summarized, some new results are presented, and several useful applications of wave energy and medical instruments are discussed.**

I. Introduction

HEALTH OFFICIALS and medical personnel have recently been confronted with several problems associated with wave propagation effects in tissues and living systems such as man. They have turned to the engineering profession for help, but have found engineers generally unable to provide the needed guidance. Physiologists and biologists have attempted to fill this void, with results that clearly demand an informed engineering critique. It seems curious indeed that although some of the early fundamental experiments with light and electromagnetic waves were performed over 100 years ago, the application of these energy forms to man himself is pitifully inadequate. This paper is presented in an attempt to define the overall problem in some small measure, and illustrate the new applications methodology and techniques. It quite frankly represents an attempt to stimulate the engineering profession to respond to this urgent medical and social need.

The paper consists of two basic parts. Section II describes electromagnetic radiation from, say, 1 MHz to 300 GHz, where the wavelength is large compared to cell sizes. There is little scattering, thus most of the wave reflection and transmission line concepts are applicable. Section III describes radiation effects from the far infrared through the ultraviolet spectrum. Here there is significant wave scattering and molecular absorption effects, which require different theoretical and experimental approaches.

Manuscript received February 24, 1972; revised March 20, 1972. *This invited paper is one of a series planned on topics of general interest—The Editor.* Facilities and administrative support for the research described were provided by Social Rehabilitation Service Research and Training Grant 16-P-56818/0-09; Bureau of Radiological Health Grant 8-RO1-RL00528-02; National Institutes of Health Grants GM-16436 and GM-16000; and the Department of Rehabilitation Medicine, Department of Electrical Engineering, and Center for Bioengineering at the University of Washington, Seattle.

The authors are with the Department of Electrical Engineering, Department of Rehabilitation Medicine and Center for Bioengineering, University of Washington, Seattle, Wash. 98195.

II. Radio Frequency and Microwave Effects

A. Introduction

Electromagnetic fields in the spectrum between 1 MHz and 100 GHz have special biological significance since they can readily be transmitted through, absorbed by, and reflected at biological tissue boundaries in varying degrees, depending on body size, tissue properties, and frequency. There is very little scattering by tissues in this frequency range. These characteristics can result in either medically beneficial effects or biological damage or harm, depending on the circumstances. The frequency range receiving the most attention in terms of biological interaction is in the microwave spectrum of 300 to 10 000 MHz. This is due to the widespread use of high-energy densities in highly populated areas and to the better absorption characteristics in the tissues of man in this frequency range.

The effect of microwaves on the biological system may be categorized into two major areas, one involving medically beneficial effects and the other involving harmful effects. The effects may be further classified as either thermal effects resulting from high-level microwave power or low-level effects that may or may not be a thermal effect. To the uninitiated, a glance at the present state of knowledge in this area will provide a confusing picture indeed! One will see microwave power densities up to 590 mW/cm² being used in clinics for routine diathermy treatment of many areas of the human body [1], [2], and units of refrigerated human whole blood at 4°C brought up to body temperature within a minute, for immediate transfusion, by microwave heating [3]. One will also see research on the application of high-power microwave energy for treatment of cancer [4] and for quickly eliminating hypothermia after open heart surgery. Yet at the same time we note that the maximum recommended safe power density for long-term human exposure varies from 10 mW/cm² in the United States to as low as 0.01 mW/cm² in the USSR. We hear strong arguments between the microwave oven industry, the military, and the Public Health Service, and also between reputable scientists, on where realistic safety levels for microwave exposure should lie. The most recent and most intense public concern stems from both the passage of the Radiation Control for Health and Safety Act of 1968 [5], [6], and the increasing sales of microwave ovens [7]. This coupled with conflicting results from the past research done in the United States and the USSR, and inadequate quantitative data on biological effects

Reprinted from *Proc. IEEE*, vol. 60, pp. 692–718, June 1972.

of microwaves, has raised many questions that remain unanswered. Fortunately, with the current public concern with radiation safety, an increasing number of electromagnetic engineers are becoming interested in studies on both biological effects and safe medical applications of electromagnetic energy. This new interest should result in a better quantitative understanding of the mechanisms of interaction.

B. Observed Effects in Tissue

1) Thermal Effects: The most investigated and documented effect of RF power on biological tissues is the transformation of energy entering the tissues into increased kinetic energy of the absorbing molecules, thereby producing a general heating in the medium. The heating results from both ionic conduction and vibration of the dipole molecules of water and proteins. The power absorbed by the tissues will produce a temperature rise that is dependent on the cooling mechanisms of the tissue. The patterns of the fields producing the heating are complex functions of the frequency, source configuration, tissue geometry, and dielectric properties of the tissues. The temperature patterns are further modified by the thermal properties of the tissues and neurocirculatory mechanisms. When the thermoregulatory capability of the system or parts of the system is exceeded, tissue damage and death can result. This occurs at absorbed power levels far above the metabolic power output of the body. Death usually results from the diffusion of heat from the irradiated portion of the body to the rest of the body by the vascular system. As the absorbed energy steadily increases, the protective mechanisms for heat control break down, resulting in an uncontrolled rise in body temperature. Michaelson [8]–[10] has demonstrated these effects in dogs and rats.

The absorption or heating patterns induced by radiation of the biological system will be nonuniform and dependent on the dielectric properties of the tissues. The absorption is high and the depth of penetration low in tissues of high water content such as muscle, brain tissue, internal organs, and skin, while the absorption is an order of magnitude lower in tissues of low water content such as fat and bone. Reflections between interfaces separating tissues of high and low water content can produce severe standing waves accompanied by "hot spots" that can be maximum in either tissue, regardless of dielectric constant or conductivity. Skin burns over the rib cage of test animals exposed to microwave power are examples of this. Local lesions of the skin and underlying tissues due to thermal effects from microwave exposure have been observed. These microwave burns tend to be deep, like fourth-degree burns, due to the deep penetration of the energy. Tissues with poor blood circulation or temperature regulation such as the lens of the eye, the gall bladder, and parts of the gastorintestinal tract are vulnerable. Experiments have shown that severe and injurious selective temperature increases can occur in these tissues with only slight increases in rectal and oral temperature. Injurious effects may occur at different temperatures depending on the tissue. For instance, it is well known that the testes undergo degenerative changes when maintained at normal body temperature over a long period of time. Microwave radiation has produced damage of the testes by increasing the temperature of the glands to as little as 35°C [11].

The heating characteristic of RF power has been used for nearly three quarters of a century by the medical profession to provide deep heating for therapeutic purposes. The therapeutic temperature range of 43°C to 45°C is very close to the temperature range where destructive changes can occur. This therapeutic technique called diathermy is discussed in great detail in the literature by Schwan [2], Scott [12], Moor [1], Krusen *et al.* [13], and Lehmann [14]. Local effects of diathermy include increases in blood flow owing to arteriolar and capillary dilation, increases in filtration and diffusion across biologic membranes, and possible greater capillary membrane permeability with resulting escape of plasma proteins. Vigorous heating can result in cellular responses associated with an inflammatory reaction. Enzyme reactions can take place due to changes in metabolic rate and proteins may be denatured with resulting products such as polypeptides and histamine-like substances becoming biologically effective. Diathermy has altered the physical properties of fibrous tissues in tendons, joint capsules, and scars to allow them to yield much more to stress. Other effects are relaxation of muscle spasms and increases in pain threshold of nerves.

2) Nonthermal Effects: The term "nonthermal effect" generally relates to an effect that is not associated with an increase in temperature. One such effect, observed by Herrick [15], Heller [16], and Heller *et al.* [17], [18], as well as Wildervank *et al.* [19], is due to forces acting on particles and is called the pearl chain effect. This effect is seen when suspended particles of charcoal, starch, milk, erthrocytes, or leucocytes (blood cells) are placed in a continuous or pulsed RF field in the range of 1–100 MHz. The particles form into chains parallel to the electric lines of force. For each particle type there is a frequency range where the effect occurs at minimum field strength. The chain formation, quantified by Satio *et al.* [20], [21], and Furedi *et al.* [22], [23], is due to the attraction between particles in which dipole charges are induced by the RF fields. The effect is discussed in detail by Schwan [2] and Presman [24]. Schwan has indicated that the effect occurs in biologic tissue at field levels where damaging thermal effects will occur.

Another nonthermal effect is the dielectric saturation occurring in solutions of proteins and other biological macromolecules due to intense microwave fields. It is suggested by Schwan [25] that such fields can cause polarized side chains of the macromolecules to line up with the direction of the electric field, leading to a possible breakage of hydrogen bonds and to alterations of the hydration zone. Such effects can cause denaturation or coagulation of molecules which was confirmed experimentally by Fleming *et al.* [26]. Resonance absorption in living cells is considered to be such an effect [27]–[29], but it is doubted by some investigators that it can occur at nonthermal power levels. Paramagnetic resonance analysis is used to determine dipole movement of protein molecules to elucidate the structure of crystalline proteins [30]. Field effects in water and protonic semiconductors in biological materials are reported [31]. Organisms such as bacteria, planaria, and snails react to weak electric and magnetic fields [32], [33]. Neuromuscular responses occur in birds in electromagnetic fields [34]. A very interesting phenomenon is the hearing of sounds corresponding to the frequency of modulation by people exposed to radar beams of low average power [35]–[37]. Direct and indirect effects on the central nervous systems (CNS) have been reported by the Soviets at levels below 10 mW/cm^2 [38]–[40]. They state that the CNS is the most sensitive of all body systems to microwaves at intensities below thermal thresholds. They

TABLE I

PROPERTIES OF ELECTROMAGNETIC WAVES IN BIOLOGICAL MEDIA

		Muscle, Skin, and Tissues with High Water Content							
						Reflection Coefficient			
						Air–Muscle Interface		Muscle–Fat Interface	
Frequency (MHz)	Wavelength in Air (cm)	Dielectric Constant ϵ_H	Conductivity σ_H (mho/m)	Wavelength λ_H (cm)	Depth of Penetration (cm)	r	ϕ	r	ϕ
1	30000	2000	0.400	436	91.3	0.982	+179		
10	3000	160	0.625	118	21.6	0.956	+178		
27.12	1106	113	0.612	68.1	14.3	0.925	+177	0.651	−11.13
40.68	738	97.3	0.693	51.3	11.2	0.913	+176	0.652	−10.21
100	300	71.7	0.889	27	6.66	0.881	+175	0.650	−7.96
200	150	56.5	1.28	16.6	4.79	0.844	+175	0.612	−8.06
300	100	54	1.37	11.9	3.89	0.825	+175	0.592	−8.14
433	69.3	53	1.43	8.76	3.57	0.803	+175	0.562	−7.06
750	40	52	1.54	5.34	3.18	0.779	+176	0.532	−5.69
915	32.8	51	1.60	4.46	3.04	0.772	+177	0.519	−4.32
1500	20	49	1.77	2.81	2.42	0.761	+177	0.506	−3.66
2450	12.2	47	2.21	1.76	1.70	0.754	+177	0.500	−3.88
3000	10	46	2.26	1.45	1.61	0.751	+178	0.495	−3.20
5000	6	44	3.92	0.89	0.788	0.749	+177	0.502	−4.95
5800	5.17	43.3	4.73	0.775	0.720	0.746	+177	0.502	−4.29
8000	3.75	40	7.65	0.578	0.413	0.744	+176	0.513	−6.65
10000	3	39.9	10.3	0.464	0.343	0.743	+176	0.518	−5.95

further state that there is a reaction of the nervous system to microwave energy on skin receptors or brain cells. The Soviets also claim nonthermal effects on the cardiovascular system, including decreased arterial pressure and heart rate [30]. As a result of these interactions, they have set their level of safe exposure 1000 times lower than that of the United States. Some of the Soviet work appears to be corroborated by investigators in the United States. For example, Frey [41], [42] has observed changes in CNS activity in animals and auditory effects in humans due to very low incident power levels. Korbel [43], [44] also reports behavioral effects in white rats exposed to low levels of microwave power. These CNS and behavioral effects are the source of a great deal of controversy at the present time.

C. Theoretical Description

In order to understand some of the characteristics of radio-frequency and microwave interactions with biological materials, a list of some important wave parameters is given in Tables I and II. The first column lists selected frequencies between 1 MHz and 10 GHz. The frequencies of 27.12, 40.68, 433, 915, 2450, and 5800 are significant since they are used for industrial, scientific, and medical heating processes. The frequencies of 27.12, 915, and 2450 are used for diathermy purposes in the United States, whereas only 433 MHz is authorized in Europe for these purposes. The second column tabulates the corresponding wavelength λ in air, and the remaining columns pertain to the wave properties of a tissue group. Table I gives data for muscle, skin, or tissues of high water content, while Table II is for fat, bone, and tissues of low water content. Other tissues containing intermediate amounts of water such as brain, lung, bone marrow, etc., will have properties that lie between the tabulated values for the two listed groups. The tables list the dielectric properties, the depth of penetration, and the reflection characteristics of various tissues exposed to electromagnetic waves as a function of frequency.

1) Dielectric Properties: The dielectric behavior of the two groups of biological tissues tabulated in Tables I and II has been evaluated most thoroughly by Schwan and his associates [45]–[47] and by other researchers including Cook [48]–[50] and Cole [51]. The interaction of electromagnetic wave fields with biological tissues is related to these dielectric characteristics. The tissues are composed of cells encapsulated by thin membranes containing an intracellular fluid composed of of various salt ions, polar protein molecules, and polar water molecules. The extracellular fluid has similar concentrations of ions and polar molecules, though some of the elements are different.

The action of electromagnetic fields on the tissues produces two types of effects that control the dielectric behavior. One is the oscillation of the free charges or ions and the other the rotation of dipole molecules at the frequency of the applied electromagnetic energy. The first gives rise to conduction currents with an associated energy loss due to electrical resistance of the medium, and the other affects the displacement current through the medium with an associated dielectric loss due to viscosity. These effects control the behavior of the complex dielectric constant $\epsilon^*/\epsilon_0 = (\epsilon' - j\epsilon'')$, where ϵ_0 is the permittivity of free space, ϵ^* is the complex permittivity, ϵ' is the dielectric constant, and ϵ'' is the loss factor of the medium. The effective conductivity σ (due to both conduction currents and dielectric losses) of the medium is related to ϵ'' by $\epsilon'' = \sigma/\omega\epsilon_0$ and the loss tangent is given by $\tan\delta = \epsilon''/\epsilon' = \sigma/\omega\epsilon'\epsilon_0$. The quantity ϵ^* will be dispersive due to the various relaxation processes associated with polarization phenomena. These are indicated by the dielectric properties given in Tables I and II. The decrease in dielectric constant ϵ_H and increase in conductivity σ_H for tissues of high water content with increasing frequency is due to interfacial polarization across the cell membranes. The cell membranes, with a capacity of approximately 1 μF/cm^2, act as insulating layers at low frequencies so that currents flow only in the extracellular medium, accounting for the low conductivity of the tissues. At sufficiently low frequencies, the charging time constant is small enough to completely charge and discharge the membrane during a single cycle, resulting in a high tissue capacitance and therefore a high dielectric constant. When frequency is increased, the capacitive reactance of the cell decreases, resulting in increasing currents in the intracellular

TABLE II

PROPERTIES OF ELECTROMAGNETIC WAVES IN BIOLOGICAL MEDIA

		Fat, Bone, and Tissues with Low Water Content							
						Reflection Coefficient			
						Air–Fat Interface		Fat–Muscle Interface	
Frequency (MHz)	Wavelength in Air (cm)	Dielectric Constant ϵ_L	Conductivity σ_L (mmho/m)	Wavelength λ_L (cm)	Depth of Penetration (cm)	r	ϕ	r	ϕ
1	30000								
10	3000								
27.12	1106	20	10.9–43.2	241	159	0.660	+174	0.651	+169
40.68	738	14.6	12.6–52.8	187	118	0.617	+173	0.652	+170
100	300	7.45	19.1–75.9	106	60.4	0.511	+168	0.650	+172
200	150	5.95	25.8–94.2	59.7	39.2	0.458	+168	0.612	+172
300	100	5.7	31.6–107	41	32.1	0.438	+169	0.592	+172
433	69.3	5.6	37.9–118	28.8	26.2	0.427	+170	0.562	+173
750	40	5.6	49.8–138	16.8	23	0.415	+173	0.532	+174
915	32.8	5.6	55.6–147	13.7	17.7	0.417	+173	0.519	+176
1500	20	5.6	70.8–171	8.41	13.9	0.412	+174	0.506	+176
2450	12.2	5.5	96.4–213	5.21	11.2	0.406	+176	0.500	+176
3000	10	5.5	110–234	4.25	9.74	0.406	+176	0.495	+177
5000	6	5.5	162–309	2.63	6.67	0.393	+176	0.502	+175
5900	5.17	5.05	186–338	2.29	5.24	0.388	+176	0.502	+176
8000	3.75	4.7	255–431	1.73	4.61	0.371	+176	0.513	+173
10000	3	4.5	324–549	1.41	3.39	0.363	+175	0.518	+174

medium with a resulting increase in total conductivity of the tissue. The increase in frequency will also prevent the cell walls from becoming totally charged during a complete cycle, resulting in a decrease in ϵ_H. At a frequency of approximately 100 MHz and above, the cell membrane capacitive reactance becomes sufficiently low that the cells can be assumed to be short-circuited. In the frequency range of 100 MHz to 1 GHz, the ion content of the electrolyte medium has no effect on the dispersion of the dielectric constant so the values of ϵ_H and σ_H are relatively independent of frequency. Schwan [45], [52] has suggested, however, that suspended protein molecules with a lower value of dielectric constant act as "dielectric cavities" in the electrolyte, thereby lowering the dielectric constant of the tissue. He attributes the slight dispersion of ϵ_H to the variation of the effective dielectric constant of the protein molecules with frequency. The final decline of ϵ_H and increase of σ_H at frequencies above 1 GHz can be attributed to the polar properties of water molecules which have a relaxation frequency near 22 GHz.

The dielectric behavior of tissues with low water content is quantitatively similar to tissues with high water content, but the values of dielectric constant ϵ_L and conductivity σ_L are an order of magnitude lower and are not quantitatively understood as well. This is due to the fact that the ratio of free to various types of bound water is not known. There is also a large variation in tissues of low water content. Since water has a high dielectric constant and conductivity compared to fat, the net tissue dielectric constant and conductivity will change significantly with small changes in water content.

The values of ϵ and σ will also vary with temperature. In the microwave region, where dispersion is small, the variation is given by

$$\frac{\Delta\sigma}{\sigma} = 2\%/^\circ\text{C}$$

and

$$\frac{\Delta\epsilon}{\epsilon} = -0.5\%/^\circ\text{C}.$$

The dielectric properties of the tissues play an important part in determining the reflected and transmitted power at interfaces between different tissue media. They also determine the amount of total power a given biological specimen will absorb when placed in an electromagnetic field.

2) Propagation and Absorption Characteristics of Waves

a) Plane tissue layers exposed to plane waves: Plane wave propagation characteristics in plane layered biological tissues may be examined to show how radiation is absorbed when the radius of curvature of the tissue surface is large compared to a wavelength. The propagation constant $k_{H,L}$ for power transmission through biological tissues can be written in terms of the complex dielectric constants $\epsilon_{H,L}^*$ and free space propagation constant k_0 in the standard form

$$k_{H,L} = k_0(\epsilon_{H,L}^*/\epsilon_0)^{1/2} = \beta_{H,L} - j\alpha_{H,L} \qquad (1)$$

where the wavelengths $\lambda_{H,L} = 2\pi/\beta_{H,L}$ are significantly reduced in the tissues due to the high dielectric constants. Tables I and II indicate that the factors of reduction are quite large, between 6.5 and 8.5, for tissues of high water content, and between 2 and 2.5 for tissues with low water content. In addition to the large reduction in wavelength, there will be a large absorption of energy in the tissue which can result in heating. The absorbed power density $P_{H,L}$ resulting from both ionic conduction and vibration of dipole molecules in the tissues is given by

$$P_{H,L} = \frac{\sigma_{H,L}}{2} |E|^2 \qquad (2)$$

where E is the magnitude of the electric field. One may note from the conductivities listed in Tables I and II that absorption in tissue of higher water content may be as high as 60 times greater than in that of low water content for the same electric fields. The absorption of microwave power will result in a progressive reduction of wave power density as the waves penetrate into the tissues. We can quantify this by defining a depth of penetration $d = 1/\alpha$ or a distance that the propagating wave will travel before the power density decreases by a factor of e^{-2}. We can see from Tables I and II that

the depth of penetration for tissues of low water content is as much as 10 times greater than the same parameter for tissues of high water content.

Since each tissue in a complex biological system such as man has different complex permittivity, there will in general be reflections of energy between the various tissue interfaces during exposure to microwaves. The complex reflection coefficient due to a wave transmitted from a medium of complex permittivity ϵ_1^* to a medium of permittivity ϵ_2^* and thickness greater than a depth of penetration is given by

$$\rho = re^{j\phi} = \frac{\sqrt{\epsilon_1^*} - \sqrt{\epsilon_2^*}}{\sqrt{\epsilon_1^*} + \sqrt{\epsilon_2^*}}. \quad (3)$$

The values r and ϕ for various interfaces are tabulated in Tables I and II. Note the large reflection coefficient for an air–muscle or a fat–muscle interface. When a wave in a tissue of low water content is incident on an interface with a tissue of high water content of sufficient thickness (greater than the depth of penetration), the reflected wave is nearly 180° out of phase with the incident wave, thereby producing a standing wave with an intensity minimum near the interface. If the wave is propagating in a tissue of high water content and is incident on a tissue of low water content, the amplitude of the reflected component is in phase with the incident wave, thereby producing a standing wave with an intensity maximum near the interface. If there are several layers of different tissue media with thicknesses less than the depth of penetration for each medium, the reflected energy and standing wave pattern are influenced by the thickness of each layer and the various wave impedances. These effects may be obtained from the standard transmission line equations. The distribution of electric field strength E in a given layer is

$$E = E_0[e^{-jkz} + \rho e^{jkz}] \quad (4)$$

where E_0 is the peak magnitude of the field and ρ is the reflection coefficient. From (3), the equation for absorbed power density in the tissue layer, we obtain

$$P = \frac{\sigma E_0^2}{2}[e^{-2\alpha z} + r^2 e^{2\alpha z} + 2r\cos(2\beta z + \phi)]. \quad (5)$$

Schwan [2], [45] has made extensive calculations of these absorption distributions in various tissues. Typical distributions are shown in Fig. 1 for a wave transmitted through a subcutaneous fat medium into a muscle medium. The absorption is normalized to unity in the muscle at the fat–muscle interface. The relative absorption curves shown are not changed for smaller fat thicknesses. The severe discontinuity between the absorbed power in the muscle and that in the fat is quite apparent. Also, it can be seen that the standing wave peaks become larger in the fat and the wave penetration into the muscle becomes less with increasing frequency. This illustrates clearly the desirability for using frequencies lower than the 2450-MHz allocation for diathermy. Subcutaneous fat may vary from less than a centimeter in thickness to as much as 2.5 cm in thickness for different individuals. Deep heating for diathermy requires the transmission of energy through this subcutaneous fat layer to the muscle layer. Optimum results are attained with maximum heating in the muscle. The absolute values of absorbed power density in the tissue layers are dependent on incident power density, skin thickness, and fat thickness. Fig. 2 illustrates the absorbed power density at the muscle interface and the peak absorbed power density in a skin layer 2 mm thick as a function of fat thickness for an incident power density of 1 mW/cm². These values may be used to determine the absorbed power at other locations in the muscle and fat by relating them to the curves in Fig. 1. The peak absorbed power density is always maximum in the skin layer for the plane layered model. This is significant since the thermal receptors of the nervous system are located there and will indicate pain when the incident power density reaches levels that could thermally damage the tissue. With surface cooling of the skin, however, by natural environmental conditions or by controlled clinical procedures, the temperature increases may be higher in the fat or muscle. The peak absorption in the various tissues may vary over a wide range with fat thickness and frequency. It is apparent that frequencies below 918 MHz can penetrate more deeply into the tissues. The implications of this in terms of both radiation hazards and therapeutic applications are apparent. The first two figures clearly indicate the advantages of lower frequencies for diathermy, including 1) increased penetration into the muscle tissue, 2) less severe standing waves and resulting "hot spots" in the fat, and 3) better control and knowledge of the ab-

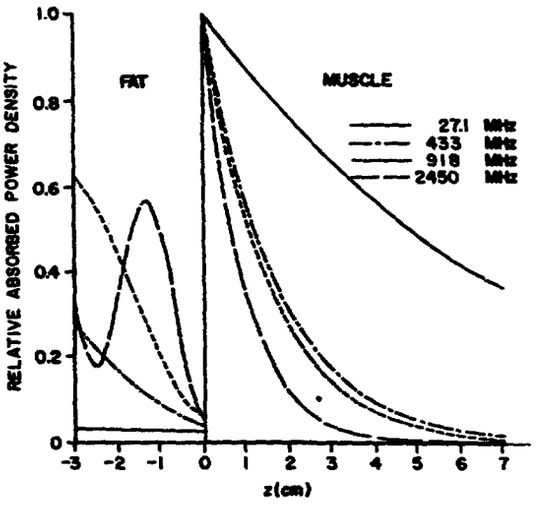

Fig. 1. Relative absorbed power density patterns in plane fat and muscle layers exposed to a plane wave source.

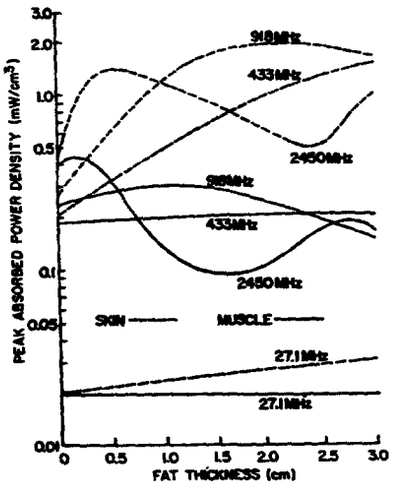

Fig. 2. Peak absorbed power density in plane skin and muscle layers as a function of fat thickness.

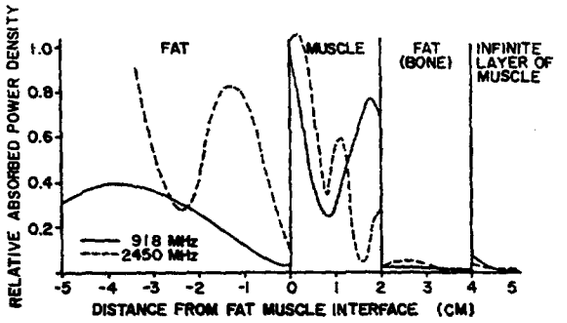

Fig. 3. Relative absorbed power density patterns in plane fat, muscle, and bone layers exposed to a plane wave source.

sorbed energy for a given incident power for a large variation of fat thicknesses between different patients.

There is a practical lower limit, however, on the frequency that can be used. As the frequency is decreased, the applicator needed becomes increasingly large until it is no longer possible to obtain desired selective heating patterns. If the applicator is not increased in size as frequency is lowered, only superficial heating will result. This has been discussed in detail by Guy and Lehmann [53], and Guy [54].

A problem of interest in diathermy is the determination of how effective microwaves are in heating a layer of bone beneath a layer of subcutaneous fat and muscle. Fig. 3 illustrates heating patterns for this case using diathermy frequencies of 2450 MHz and 918 MHz for a 2-cm-thick bone. The results clearly show that the absorption in the bone is very poor due to both a severe reflection and a low electrical conductivity. Since a standing wave peak at 918 MHz occurs in the muscle near the bone surface, we would expect significant bone heating due to thermal conduction from the muscle.

b) Spherical tissue layers exposed to plane waves: Both outside and inside body geometries also influence the amount of microwave absorption by the human body. If the entire body, or a body member such as the head or arm, is illuminated by a microwave beam of large diameter, the amounts of energy absorbed by the tissues are functions of not only the tissue layer thicknesses and cross-sectional area exposed but also the size of the body or member compared to a free space wavelength and the body surface curvatures. We can illustrate the effects of body size and curvature on absorption characteristics by considering a spherical shape body composed of tissue with a high water content.

The electric fields induced in a sphere or spherical layer (shell) of tissue by an incident plane wave field can be calculated from the general vector spherical wave solutions of the wave equation

$$E = E_0 e^{j\omega t} \sum_{n=1}^{\infty} (j)^n \frac{2n+1}{n(n+1)} (a_n m_{01n} - j b_n n_{01n}) \quad (6)$$

where the functions m_{01n} and n_{01n} are defined and the coefficients a_n and b_n are obtained as described by Stratton [55, pp. 563–567]. The equations may be evaluated on a digital computer as described by Anne *et al.* [56]–[58], and Shapiro [59]. Fig. 4 illustrates the relative absorbed power density patterns (called relative heating) for a simplified homogeneous spherical model of a cat or monkey size brain and a human size brain exposed to a 1 mW/cm² plane wave source. The origin of the rectangular coordinate system used in the figures is located at the center of the sphere with wave propa-

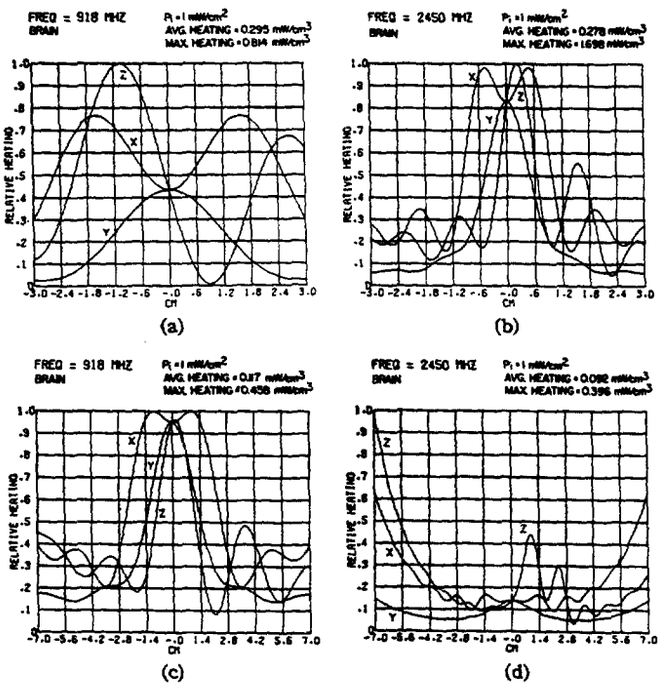

Fig. 4. Theoretical absorbed power density patterns along the x, y, and z axes models of brain tissue exposed to a plane wave source. (Incident power density 1 mW/cm², propagation along the z axis, and electrical field polarized along the x axis with origin at center of sphere.)

gation along the z axis and the E field polarized along the x axis. The maximum absorption (at the peak of the most severe standing wave) and the average absorption along the x, y, and z axes are illustrated on each plot. The dielectric properties for brain tissue used were based on values reported by Schwan [60] ($\epsilon = 35$ and 30.9, and $\sigma = 7$ and 11 mmho/cm for 918 and 2450 MHz, respectively). The figures clearly illustrate the intense fields and associated absorbed power density directly in the center of the human head and 1.2 cm off center in the animal head for 918-MHz exposure. One may note that the maximum absorption in the animal brain is larger by a factor of two than in the human brain. With 2450-MHz exposure, on the other hand, there is maximum absorption in the anterior (front) portion of the simulated human brain while there is maximum absorption in the center portion of the simulated animal brain. The animal brain receives a maximum absorption four times that of the human brain. Compared to Figs. 1–3, the plots clearly illustrate that plane tissue models cannot be used to evaluate absorbed power densities for situations where body size or radius of curvature are not large compared to a wavelength. It is significant to note that for human brain exposed to 918-MHz power, the absorption at a depth of 2.3 times the depth of penetration (depth of penetration = 3.2 cm) is twice the absorption at the surface. This corresponds to a factor greater than 200 times that expected based on the plane tissue model. At 2450 MHz, the absorbed power density at a depth approximately equal to 4.7 times the depth of penetration is 0.43 times that at the surface corresponding to a factor greater than 5000 times that expected from the plane tissue model. The regions of intense absorbed power density are due to a combination of the high refractive index and the radius of curvature of the model which produces a strong focusing of power toward the interior of the sphere which

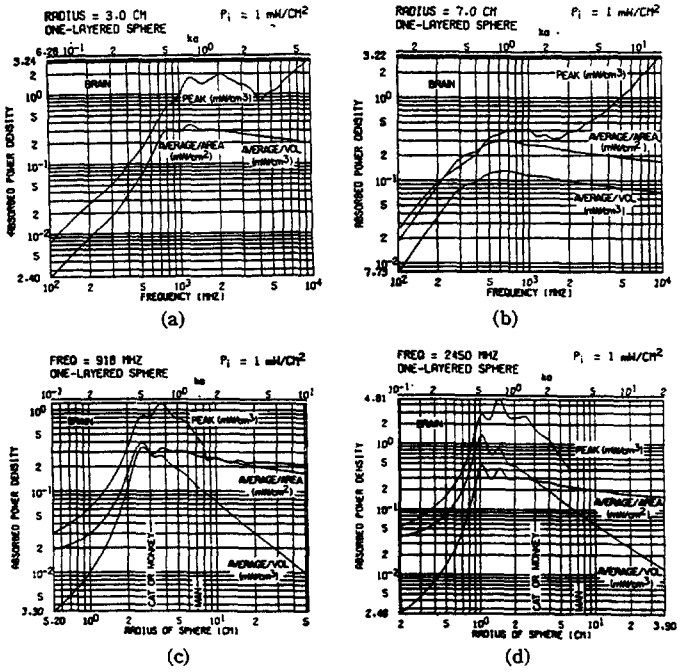

Fig. 5. Absorbed power density characteristics for spherical models of brain tissue exposed to 1 mW/cm² plane wave source.

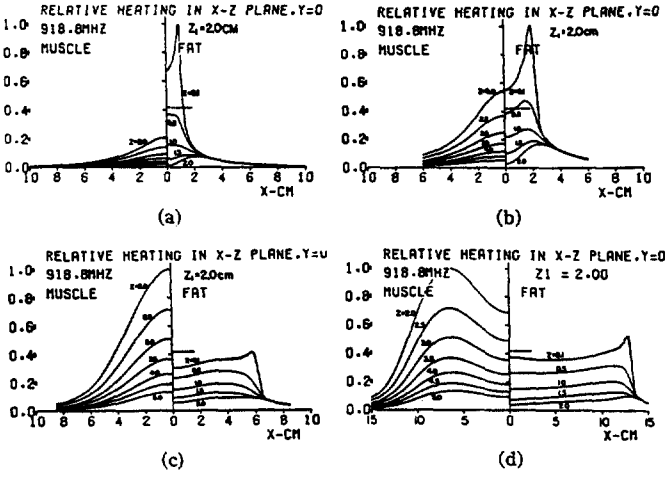

Fig. 6. Relative absorbed power density patterns in plane layers of fat and muscle exposed to TE_{10} mode waveguide aperture source with $a = 12$ cm, $f = 918.8$ MHz, and $z_1 = 2$ cm for various aperture heights. For (a)–(d) the values of b are 2, 4, 12, 26 cm, respectively.

more than compensates for transmission losses through the tissue. These results are significant in view of the many reported CNS effects at frequencies near 1 GHz. Fig. 5 illustrates the calculated peak absorbed power density per unit volume, average total absorbed power density per unit volume, and average total absorbed power density per unit area for various size spheres of brain tissue as a function of frequency. An incident power of 1 mW/cm² is assumed. Note the wide variation in absorbed power characteristics with different sphere sizes and frequencies of exposure. The graphs at the top of the figure indicate that there are sharp rises in peak absorption with increasing frequency followed by several "peaks" in the absorption curves. These peaks are related to the occurrence of "hot spots" or maxima in the internal absorption or heating patterns similar to those indicated in Fig. 4. As the frequency is further increased beyond the values where the peaks in absorption occur, the "hot spots" disappear and maximum absorption occurs at the exposed surface of the spheres. This is due to the decreasing depth of penetration with frequency. At frequencies beyond this point the peak absorption at the surface increases with frequency since the constant incident power is absorbed in a decreasingly smaller volume. The peak internal heating for the human head size sphere is maximum in the UHF frequency range centered near 915 MHz. This again is significant in terms of the large number of reported CNS effects for human exposure in the UHF frequency range. The phenomenon of hearing radar pulses is also reported in this frequency range [35], [36]. The graph indicates a further increase in peak absorption at frequencies above the UHF range, but this again is due to decreasing depth of penetration resulting in increased surface absorption. The curves at the bottom of Fig. 5 also indicate some interesting phenomena. They show that peak absorption can vary over an order of magnitude depending on brain size. The curves clearly indicate some important points to consider when one relates results between different size animals, insects, or humans exposed to RF radiation. Similar calculations have been made for muscle spheres to obtain clues to internal heating effects due to whole body radiation. Results are very similar to the curves for brain tissue given in Fig. 5. Peak absorbed power density inside the body is important since it is related to the location where localized effects or damage may occur as a function of frequency and animal size. The average absorbed power per unit volume is important because it is related to the time it takes for an exposed animal's thermoregulatory system to become overloaded or to the time that a steady-state thermal condition is reached. There is more than an order-of-magnitude variation in this value for a sphere representing man and for those representing small animals such as mice or rats. The curves depicting average power per unit area are important since they are related to the steady-state power absorption that an animal can experience without overloading its thermoregulatory system. Although the spheres are only rough approximations to actual animal bodies, they give rough approximations on how power levels for microwave effects can be extrapolated from one animal to another or to man as a function of frequency.

c) Cylindrical tissue layers exposed to plane waves: Power absorption density patterns may also be calculated for other simple tissue geometries representing portions of the anatomy. We can roughly approximate human limbs by concentric cylindrical layers of bone, muscle, fat, and skin and express the fields in each layer by an infinite series of Bessel functions of the first and second kind as discussed by Stratton [55, pp. 349–374]. For example, the electric field parallel to the z axis of the cylinder is expressed as

$$E_z = \sum_{n=0}^{\infty} 0[A_n J_n(kr) + B_n Y_n(kr)]e^{jn\theta} \qquad (7)$$

where k is the wavenumber in the medium and the coefficients A_n and B_n are obtained by expanding the plane wave source expression into a series of Bessel functions and applying boundary conditions. Similar equations may be written for the wave polarized with the magnetic field parallel to the z axis. Ho *et al.* [61] has evaluated the equations and determined the fields and absorbed power densities for cylinders corresponding to human arms and legs exposed to plane waves. The results show the same increase in muscle-to-fat

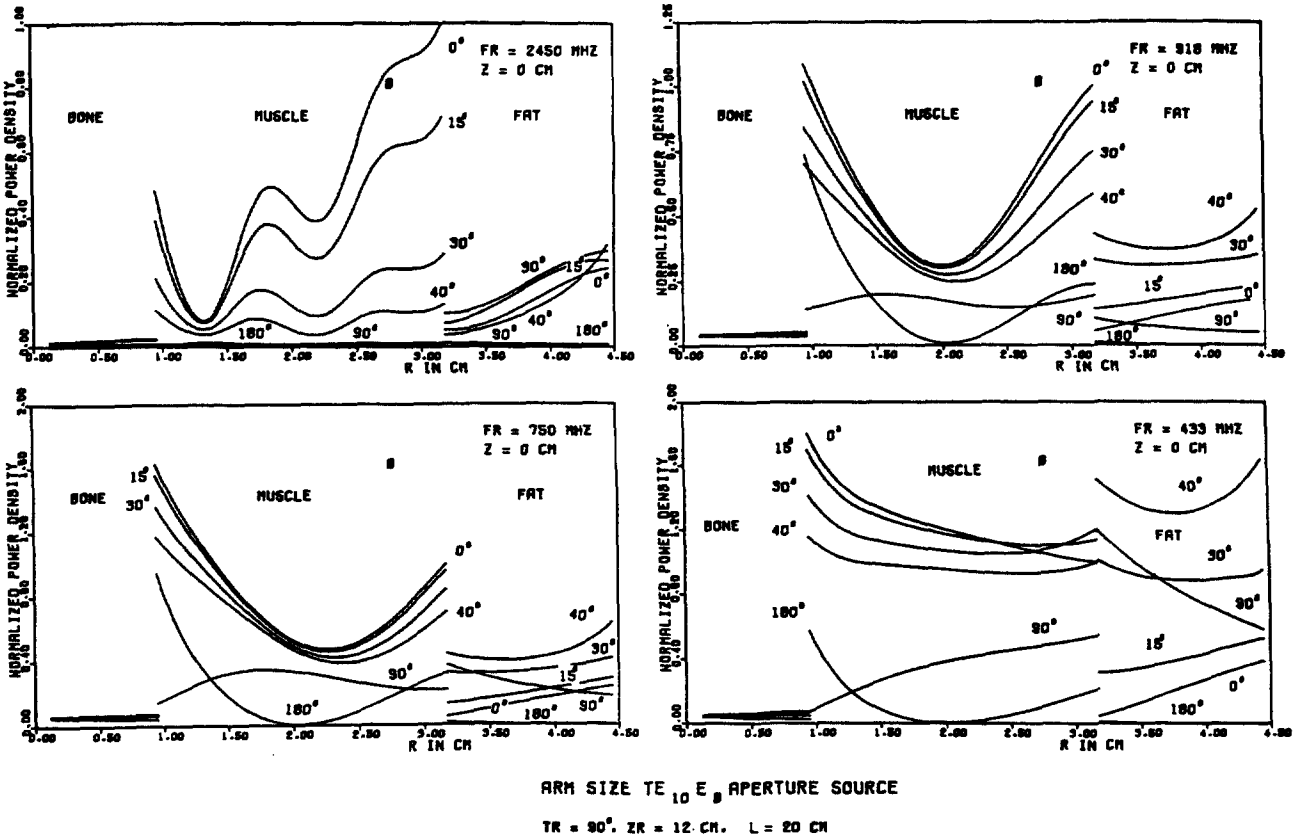

Fig. 7. Heating patterns in a cylindrical model of human arm due to a direct contact cylindrical aperture source.

absorbed power density ratio as observed for planar models exposed to lower frequency. The results also show a greater depth of energy penetration into the muscle due to the curvature of the tissues.

d) Tissues exposed to near-zone fields: If other than a plane wave source is used to expose biological tissues, the absorbed power density patterns are also very dependent on source size and distribution. Many applications of microwave power in medicine and studies on the biological effects of microwave power require an understanding of the absorbed power patterns due to tissues exposed to aperture and waveguide sources. Guy [54] has analyzed the case where a bilayered fat and muscle tissue layer is exposed to a direct contact aperture source of width a and height b. A fat tissue layer of thickness z_1 and dielectric constant ϵ_f^* in contact with a semi-infinite muscle tissue layer with a dielectric constant ϵ_m^* is assumed. The electric fields $E_{f,m}$ in the fat and muscle tissue may be expressed as Fourier integrals

$$E_{f,m}(x, y, z) = \frac{1}{(2\pi)^2} \int_{-\infty}^{\infty} \int_{-\infty}^{\infty} T_{f,m}(u, v, z) e^{j(ux+vy)} du dv \quad (8)$$

where $T_{f,m}$ are the Fourier transforms of the electric fields at the fat and muscle boundaries, derived from the boundary conditions at $z=0$ and $z=z_1$ in terms of the Fourier transform of the aperture

$$T_a(u, v) = \int_{-\infty}^{\infty} \int_{-\infty}^{\infty} a_z \times E_f(x, y, 0) e^{-j(ux+vy)} dx dy. \quad (9)$$

The aperture field is denoted as E_f $(x, y, 0)$ and a_z is a unit vector along the z axis. The expressions may be evaluated numerically and the absorption patterns plotted by means of a digital computer. As an example we may consider a waveguide aperture source and evaluate it as a diathermy applicator for use at 918 MHz. Fig. 6 illustrates the complete heating curves in the x–z plane for $a=12$ cm and $b=2$, 4, 12, and 26 cm. Heating at the fat surface for a plane wave exposure is denoted by the dashed line on the figures. The results show that the relative heating varies from intense superficial heating in excess of that produced by a plane wave to deep heating greater than produced by a plane wave as aperture size is increased.

The absorbed power density patterns in multilayered cylindrical tissues exposed to an aperture source can also be determined by using a summation of three-dimensional cylindrical waves, expressing the aperture field as a two-dimensional Fourier series and matching the boundary conditions. Ho *et al.* [62], [63] has calculated the absorbed patterns for a number of different aperture and cylinder sizes. Typical results are shown in Fig. 7 for a human arm-size cylinder exposed to a surface aperture source 12 cm long in the direction of the axis. The patterns are plotted as a function of radial distance from the center of the cylinder for various circumferential angles ϕ from the center of the aperture. The patterns are normalized to the values at $\phi=0°$ at the muscle interface. The difference between the patterns in the cylindrical tissues and those illustrated for the plane layers indicates the importance of tissue curvature when assessing the effectiveness and safety of devices designed for medical application of microwave energy.

All of the theoretical results discussed in this section strongly point to the ineffectiveness of the 2450-MHz frequency as a diathermy frequency as pointed out in earlier reports by Schwan [45], [46], Lehmann [14], [65], and Guy

[54], [65]. Although the lower frequencies of 915 MHz authorized in the United States or 433 MHz authorized in Europe appear to be better choices, it appears from the theoretical data that 750 MHz would be the best choice. By their nature the frequencies that provide the best therapeutic heating would also be frequencies that could be most hazardous to man in an uncontrolled situation.

D. Measurements in Biological Tissues

The only way that realistic tradeoffs can be made between risks of biological damage and health benefits in the use of electromagnetic energy is to have available a quantitative description of what these effects are. Without proper instrumentation or a clear understanding of how electromagnetic fields interact with the tissue on a microscopic and macroscopic scale, or on the entire body structure, it is difficult indeed to say whether an observable effect may be thermal or nonthermal in origin or is merely an artifact due to the nature of the experimental approach. It is important that investigations of these effects be conducted in such a way that all aspects of the research are quantified, including the fields induced both inside and outside the tissues; the type and degree of effect; whether the effect is harmful, harmless, or merely an artifact; whether it is a thermal or a nonthermal effect; and how it relates to the results obtained by other investigators. Body size of the experimental animal must be taken into account, along with accurate *in vivo* dosimetry, so that results from one investigator obtained from rats can be related to those from another investigator using cats, monkeys, dogs, frogs, or a tissue sample in a test tube. Since body absorption cross sections and internal heating patterns can differ widely, as evidenced in the discussion in the last section, an investigator may think he is observing a low level or a nonthermal effect in one animal because the incident power is low while in actuality the animal may be exposed to as much absorbed power in a specific region of the body as another larger animal is with much higher incident powers.

Fig. 8 illustrates some of the problems encountered in measuring the fields and related effects in biological systems. Here we consider a controlled experiment in which an animal is exposed to a laboratory radiation source and we wish to see what the implication of observable biological effects is to a human exposed to some arbitrary source. For the human it is customary and desirable to define the hazard in terms of an incident power flux density or an electric field amplitude (denoted by I) as measured with a survey meter without the presence of the subject. When the subject enters the environment, however, many complicating factors arise. These include an unknown amount of scattered power (denoted by S) and transmitted power (denoted by T) and internal reflections (denoted by R). The survey meter will not give an accurate indication of the incident field I or the absorbed fields under these circumstances. Standing waves will occur on the outside of the man which may give a wide range of different readings on the survey meter, depending on its position. The greatest complicating factors are the result of interference patterns within the tissues, resulting in regions of intensification of absorbed power or hot spots and also regions of low absorbed power. These absorbed power patterns will vary depending on the source, frequency, body size, and geometry and the environment around the subject as described in the previous section.

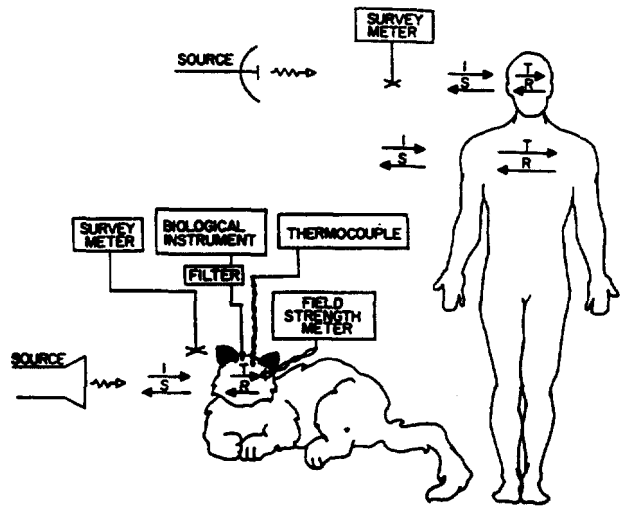

Fig. 8. Instrumentation associated with man and test animals exposed to electromagnetic radiation.

The only practical way to quantify biological damage accurately in terms of incident power levels for establishing safety standards for humans is through animal experimentation or irradiation of biological specimens *in vitro*. The question is how do we relate the biological effects to the fields and extrapolate the results to the establishment of safety standards for humans. In the controlled animal or biological tissue experiment we have the option to set up any field configuration we desire, where an effective power density can be determined with a survey meter. We cannot assume, however, that if a certain power density level produces quantifiable effects of damage in the animal or specimen, similar effects can take place in the human with the same effective incident power. With the animal or specimen there is scattering, absorption, and internal reflections uniquely associated with the animal's body and tissue characteristics or the specimen geometry which result in an absorbed power density pattern different from that for the case of human exposure. The approach that makes most sense is to quantify the actual fields, current density, or absorbed energy density in the tissues or specimen and relate this to the biological effects or damage that may occur. There has been some question among investigators concerning the most meaningful parameters to measure and how to relate them between the experimental animal and man. Bowman [66] has discussed the problem in great detail and suggests the measurement and use of the square of the magnitude of the electric field $|E|^2$ or energy density $U_E = \frac{1}{2}\epsilon' |E|^2$ as the most useful parameters to quantify hazards. He suggests the measurement of $|E|^2$ with implanted dipole antennas. Schwan [67], on the other hand, proposes that current density in the tissues is the most useful parameter to relate to the hazards. In this paper we propose the use of the absorbed power density as the most useful parameter since it is related directly to the well-established thermal effects or damage that may occur. It really makes no difference which of the above parameters are chosen, since they are all directly proportional to the magnitude or the square of the magnitude of the electric field in the tissues. One may measure these parameters directly by implanted dipoles and thermocouples, or indirectly by thermography, and relate them to electrophysiological phenomena measured while the test animal is exposed to radiation. Once this in-

formation is available, the next task is to determine what incident power or external field intensity, whether predominantly a radiation field, electric field, or magnetic field, will produce the same effect in man. The essentials to know, then, are the following: 1) what level of power per gram or unit volume absorbed in the tissue of an animal or specimen will produce an effect or damage; and 2) what level of incident power or fields as measured by a survey meter will produce the same absorbed power in the tissues of a human. These questions can be answered only through the use of sound measurement techniques. The instrumentation for measuring fields and absorbed power within the tissues must not modify the field in any way. Similarly, sensors for measuring biological variables must not modify the fields or be susceptible to interference. Currently used measurement techniques are described next.

1) Radiation Survey Meters: Since the Radiation Control for Health and Safety Act was passed in 1968 [5], there has been considerable improvement in radiation survey meters for measuring radiation power densities in air. Typical designs are illustrated in Fig. 9. The meter usually consists of a sensor consisting of two orthogonal electric dipole elements, each terminated in a thermocouple or microwave diode element and coupled via small-diameter high-resistance wires to a voltmeter calibrated to record power density directly in mW/cm². A thermocouple model described by Aslan [68] consists of a pair of thin-film vacuum-evaporated electrothermic elements that function as both antenna and detector. The sensor materials are antimony and bismuth deposited on a plastic or mica substrate, all secured to a rigid dielectric material for support. The length of the dipoles is small compared to a wavelength to allow the unit to monitor power with minimum perturbation on the RF field. The dc output of the sensor is directly proportional to the RF power heating the element. The hot and cold junctions of the electrothermic element, separated by 0.75 mm, are in the same ambient environment, thereby providing an output relatively independent of ambient temperatures. With the thin-film elements oriented at 90° to each other and connected in series, the total dc output is independent or orientation and field polarization about the axis of the probe and is proportional to the square of the electric field vector. If the proportionality constant relating E to H is known or remains constant, such as 377 Ω in the far field, the output can be calibrated in terms of power density. In the near field, the meter will read an effective power density or simply the square of the electric field divided by 377. Lead wires carrying the dc output of the thermocouples are shielded with ferrite materials and maintained perpendicular to the plane of the antennas. They will therefore be invisible to the propagating wave when the antenna is placed parallel to the phase front. The dc output is connected to an electric voltmeter calibrated to read field density directly in mW/cm². The meter has an appropriate time constant to read average power when the meter is used to measure modulated RF power density. The second configuration illustrated in Fig. 9 and described in the literature by Rudge [69] is similar, except that it uses a pair of matched diodes as sensing elements. Care must be exercised with this design such that the diodes are operated in the square low range.

Survey meters of this type can be used meaningfully only to measure power density in a radiation-type field or the square of the electric field intensity in a near zone field. This information is not enough, however, to indicate what is happening in the tissues of an exposed subject.

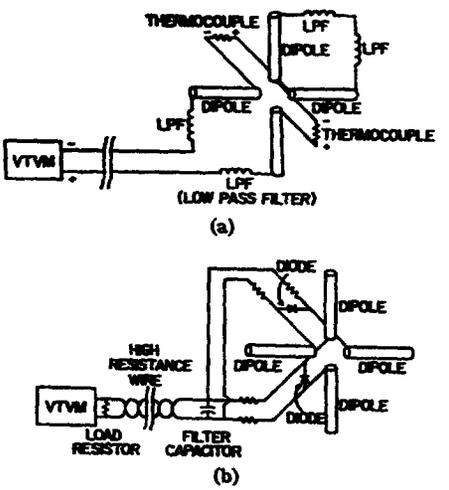

Fig. 9. Simplified sketches of various field survey meter designs. (a) Thermocouple method. (b) Diode method.

2) Measurements with Implanted Probes: One of the most vexing problems in studies involving the interaction of electromagnetic fields and living biological systems and tissues is the quantification of the fields induced in the tissues by nearby sources. Electromagnetic fields or quantities related to the fields can be measured both *in situ* and *in vivo* in test animals or even humans by means of implanted microwave diodes thermocouples or thermistors. Thermocouples and thermistors were used extensively in the past for measuring the temperature rise in tissues exposed to radiation. Osborne and Frederick [70] used thermocouples inserted into the eyes of dogs to measure temperature increases associated with microwave heating of the eyes. The thermocouples were inserted before and after the microwave exposure. Richardson [71] also used thermocouples in the eyes of rabbits to measure temperature increases associated with opacity formation by exposing the eyes to microwave radiation. Lehmann and associates [64], [72] used thermistors for measuring temperature increases in the thigh of live pigs exposed to shortwave and microwave diathermy equipment. Similar experiments were also carried out with volunteers [73], [74]. There are several problems associated with the use of thermocouples or thermistors to ascertain absorbed power: 1) the element senses only the temperature of the tissue which is also a function of other mechanisms such as thermal diffusion, blood flow, and the thermoregulatory characteristics of the animal; 2) if the sensor is left in the tissue during irradiation, it can be directly heated by the RF fields or it can significantly modify the fields and the associated temperature rises; and 3) the sensor is relatively insensitive to low-power densities.

All of these problems can be eliminated through a technique that utilizes a small diameter plastic or glass tube sealed at one end and implanted at the location where a measurement of the absorbed power is desired. The tube, illustrated in Fig. 10, is long enough so that the open end, fitted with a plastic guide, protrudes from the tissue. A very small diameter thermocouple is inserted into the tube with the sensor located at the probe tip and an initial temperature is recorded. The thermocouple is quickly withdrawn from the tube and the

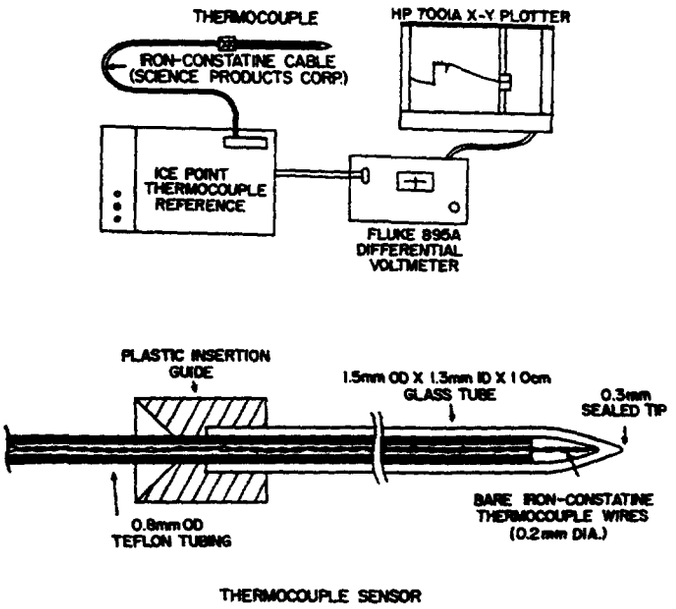

Fig. 10. Thermocouple method for power absorption density measurements *in vivo*.

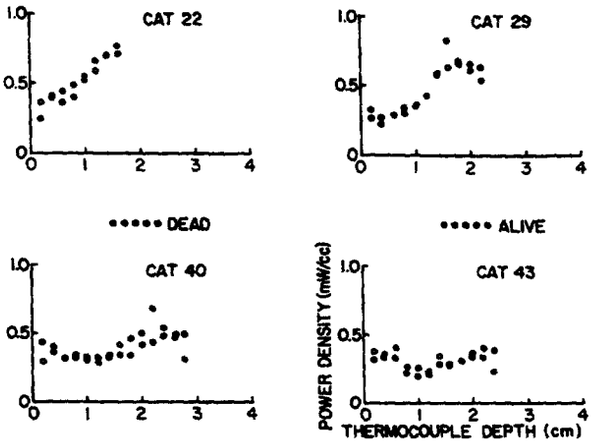

Fig. 11. Power absorption density in brain of cat exposed to 915-MHz microwave power calculated from thermocouple measurements. (Values are based on an incident power density of 2.5 mW/cm².)

animal is exposed under the normal conditions of the experimental protocol with the following exceptions. Instead of using the power level normally chosen for a given experiment, a very high power burst of radiation of duration sufficient to produce a rapid but safe temperature rise in the tissue is applied to the animal. The thermocouple is then rapidly returned to its original position and the new temperature is recorded for several minutes. The temperature versus time curve then is extrapolated back in time to the period when the power was applied and, based on the density and specific heat of the tissue, the absorbed power is calculated from the difference between initial and final extrapolated temperatures. The short exposure period insures that there is no loss of heat due to cooling or diffusion, so the expression

$$P = \frac{4.186 \rho c \Delta T}{t} \tag{10}$$

may be used to calculate the absorbed power density P in W/cm³, where ρ is the tissue density in g/cm³, c the specific heat of the tissue, ΔT the temperature change in degrees Celsius, and t the time of exposure in seconds. The measured absorbed power can then be used to relate the input power of the source to the absorbed power in the tissue under normal lower power exposure conditions. Fig. 11 illustrates power absorption profiles measured in the brains of various cats exposed to radiation. The scale corresponds to the peak absorbed power density per 2.5 mW/cm² applied to the head. Since the results are the same for both live and dead brain tissue, it is apparent that the time of exposure is sufficiently short that blood cooling effects are negligible.

The same techniques involving microwave diodes and dipoles that are used for direct measurement of the fields in air can also be used in tissues. There are difficulties, however, since the ratio of dipole length to feedline separation must be kept large to maintain accuracy while at the same time the dipole must be sufficiently short to implant with a probe. Bowman [75] proposes an implantable probe using three orthogonal dipole and diode combinations of this type with small carbon filaments as lead wires. Guy [76] has used a microwave diode, with the pigtail leads cut to ½ cm as a dipole antenna similar to that shown in Fig. 9, to make field measurements at the brain surface of a cat. The major problem with this type of sensor is that it must be calibrated for each tissue that it is placed in to account for changes in dipole source impedance. The results of using the thermocouple and diode sensors imbedded in tissues are described further in a later section. These techniques are slow and cumbersome to implement, however, and it is not always clear where to implant the probes since the regions of maximum absorbed power in the animals are generally unknown. More complete dosimetry information can be obtained by an indirect thermograph technique.

3) Measurement of Absorbed Power Density by Thermography: Guy [77] has described a method for rapid evaluation of absorbed power density in tissues of arbitrary shape and characteristics when they are exposed to various sources, including plane wave, aperture, slot, and dipoles. The method, valid for both far- and near-zone fields, involves the use of a thermograph camera for recording temperature distributions produced by energy absorption in phantom models of the tissue structures. The absorbed power or magnitude of the electric field may then be obtained anywhere on the model as a function of the square root of the magnitude of the calculated heating pattern. The phantoms are composed of materials with dielectric and geometric properties identical to the tissue structures they represent. Phantom materials have been developed which simulate human fat, muscle, brain, and bone. These materials have complex dielectric properties, illustrated in Fig. 12, that closely resemble the properties of human tissues reported by Schwan [60], where the parameters ϵ_f, ϵ_m, and ϵ_b are the dielectric constants and τ_f, τ_m, and τ_b are the loss tangents of fat, muscle, and brain tissue, respectively. The modeling material for fat may also be used for bone. The synthetic muscle can also be used to simulate other tissues with high water content. The dielectric constant can be varied over a wide range by varying the percentage of polyethylene powder which simulates protein molecules and the conductivity can be controlled by the salinity of the material. The properties of the synthetic fat can be varied over a wide range to simulate other tissues of low water content by varying the amounts of aluminum powder to control the dielectric constant and of acetylene black to control the conductivity. A simulated tissue structure composed of these modeling materials will have the same

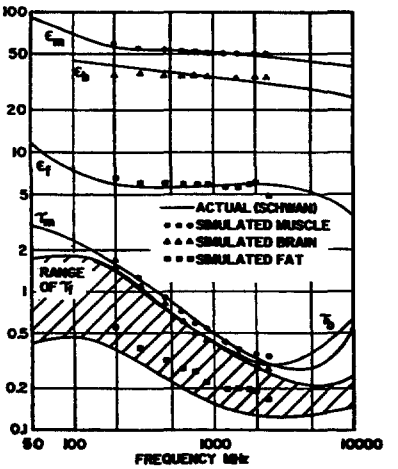

Fig. 12. Dielectric properties of actual and simulated human tissues (fat, muscle, and brain).

internal field distribution and relative heating functions in the presence of an electromagnetic source as the actual tissue structure. Phantom models of various tissue geometries can be fabricated as shown in Fig. 13. They include stratified layers of muscle and fat of various thickness, circular and irregular cylindrical structures consisting of synthetic fat, muscle, and bone, and spheres of synthetic brain to simulate various parts of the anatomy. The models are designed to separate along planes perpendicular to the tissue interfaces so that cross-sectional relative heating patterns can be measured with a thermograph. A thin 0.0025-cm-thick polyethylene film is placed over the precut surface on each half of the model to prevent evaporation of the wet synthetic tissue.

The technique for using the phantom model is now described. The model is first exposed to the same source that will be used to expose actual tissue. The power used on the model will be considerably greater, however, in order to heat it in the shortest possible time. After a short exposure, the model is quickly disassembled and the temperature pattern over the surface of separation is observed and recorded by means of a thermograph. The exposure is applied over a 5- to 60-s time interval depending on the source. After a 3- to 5-s delay for separating the two halves of the model, the recording is done within a 5-s time interval or less. Since the thermal conductivity of the model is low, the difference in measured temperature distribution before and after heating will closely approximate the heating distribution over the flat surface, except in regions of high-temperature gradient where errors may occur due to appreciable diffusion of heat.

Fig. 14 illustrates the results of applying the method to the simulated spherical brain structures described previously (refer back to Fig. 4). The thermograms at the left of Fig. 14 are *C* scans taken over the surface of the separated hemispheres where brightness is proportional to absorbed power and each division is equivalent to 2 cm. The thermograms in the middle are *B* scans taken before and after exposure to the microwave sources where vertical deflection is proportional to absorbed power along the z axis of the sphere. The thermograms at the right are also *B* scans taken along the x axis of the sphere. The graphs below the *B* scans are comparisons between the theoretical and the measured absorbed power. The results agree well, with the exception of the deviation between the theoretical and the experimental values of the large sphere exposed to 918-MHz power. This is due to the

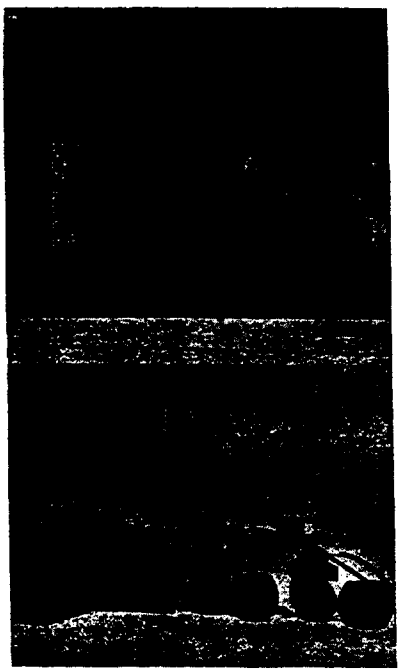

Fig. 13. Phantom tissue models.

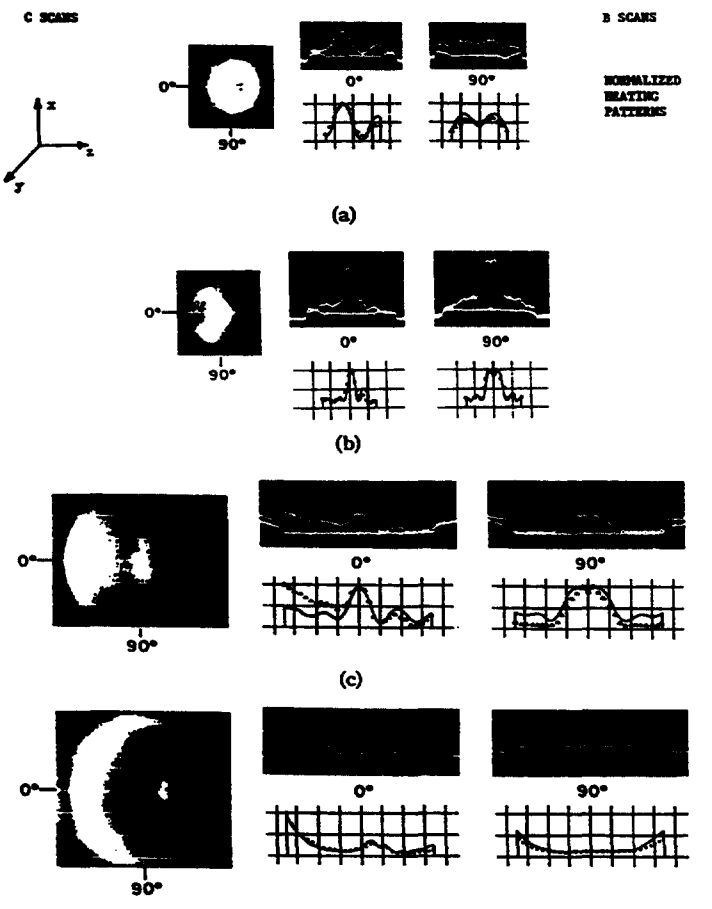

Fig. 14. Thermograms of phantom brain tissue. Scale: *C* scans, 1 div = 2 cm; *B* scans, 1 horizontal div = 2 cm, 1 vertical div = 2.5°C; and normalized patterns, 1 horizontal div = 2 cm. (Propagation in z direction with E field polarized along x axis of indicated coordinates.) (a) 6-cm diam, 918 MHz. (b) 6-cm diam, 2450 MHz. (c) 14-cm diam, 918 MHz. (d) 14-cm diam, 2450 MHz. ———, plane wave theory; · · · · ·, experimental plane wave; ▲▲▲▲▲, experimental aperture source.

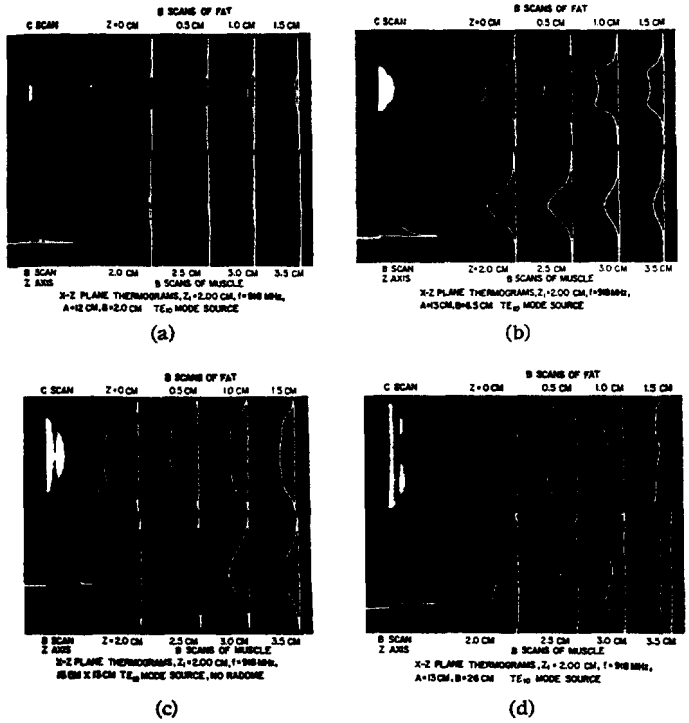

Fig. 15. Temperature distribution patterns obtained by thermography in plane layers of simulated fat and muscle exposed to a waveguide source of electromagnetic fields.

diverging fields of the finite aperture source that was used to irradiate the phantom model at this frequency.

Fig. 15 illustrates the thermograms obtained from a plane bilayered simulated fat and muscle model exposed to a waveguide source of varying height h. Since the specific heat and density of the fat is a factor 0.35 to 0.45 smaller than that of the muscle, the temperature curves in the fat ($0 \leq z_1 < 2.0$) must be reduced by this factor to be representative of absorbed power. When this reduction is made there is close correspondence between these experimental results and the theoretical results in Fig. 6. The thermograms clearly show that the fat-to-muscle heating ratio is minimized for $b = 13$ cm (b = one wavelength) and becomes excessive for aperture heights less than one-half wavelength.

The thermograph technique described for use with phantom models can also be used on test animals. The animal under test or a different animal of the same species, size, and characteristics must be sacrificed, however. The terminated animal is frozen with dry ice in the same position used for exposure conditions. It is then cast in a block of polyfoam and bisected in a plane parallel to the applied source of radiation used during the experiment. Each half of the animal is then covered with a plastic film and the bisected body is returned to room temperature. The same procedure used on the phantom model is then used with the reassembled animal to obtain absorbed power patterns over the two-dimensional internal surface of the bisected animal. Typical results are described later.

It is important to note that no metal electrodes or leads should be used to record physiological data from a region in the animal while it is being exposed to radiation. The metal leads can seriously perturb the fields in the tissues and large increases in absorbed power can occur in the tissue near the termination of the probe, as discussed in the following section. High-resistance wire leads and recording electrodes must be transparent to the fields. Also, it is necessary to filter all leads carrying physiological signals and shield the recording instrumentation to prevent the introduction of artifacts into the recording equipment. The next section describes the results of animal experiments using the techniques described in this section.

4) *Absorbed Power Measurements in a Cat Brain Exposed to 918-MHz Radiation:* An experimental protocol was developed to quantify the absorbed power and associated effects on the CNS of a cat exposed to 918-MHz microwave radiation. According to Fig. 4, similarities exist in absorbed power patterns in the CNS of test animals and humans exposed to 918-MHz radiation. Therefore, this frequency appears desirable to use for experimental testing. The experimental exposure technique and associated instrumentation are illustrated schematically in Fig. 16. Cats averaging about 2.3 kg were anesthetized with alpha-chloralose, supported in a stereotaxic instrument frame, paralyzed with Flaxedil®, and placed on artificial respiration. The radiation was directed with maximum intensity in and around the thalamic region of the brain by a controlled continuous-wave microwave power source and cavity radiator.

The response of the thalamic somatosensory area of the cat's brain to electrical stimulation of the skin on the contralateral forepaw was recorded both with and without the presence of microwave radiation. The gross thalamic electrical response was detected by means of a saline-filled glass electrode with a 6-μ-diameter tip. The electrode was placed in the thalamus and adjusted for optimum thalamic response. The electrode's position was verified in several animals by histological studies.

Metal electrodes were avoided to prevent perturbation of the microwave fields in the brain tissue. The electrode and associated reference electrodes were coupled to low-pass microwave filters by a pair of 1-mil-diameter high-resistance wires. The filter was designed to provide more than 150-dB attenuation to the microwave with no more than 20 pF of shunt capacitance to the input of a pair of field-effect transistors. The output of the transistors was fed through a processing differential amplifier to an analog tape recorder and computer of average transients. The body temperature of the cat was held constant by a heating pad connected to a rectal temperature control unit. The brain temperature was recorded during the time that the microwaves were off by placing a thermocouple in a glass pipette with a sealed tip at the homologous point in the opposite thalamus (assuming the brain was symmetrical) at the same depth as the recording electrode.

The thermocouple was removed during the exposure times to prevent any fringing field effects. The electrical response in the thalamus was recorded continuously with microwaves alternatively on and off in 15-min intervals over a total period of 8 to 12 h. The dosimetry was based on the following methods of calibration.

1) The power density in the main beam of the applicator was measured as a function of distance with a Narda model 8110 electromagnetic radiation monitor. The measurements were made for the applicator located in free space and also in the operating position on the stereotaxic support.

2) The actual field at the surface of the cat's brain was measured by means of a calibrated microwave diode coupled with high-resistance wire to a digital voltmeter shunted by a 10-kΩ resistor.

3) The temperature was measured with the thermocouple

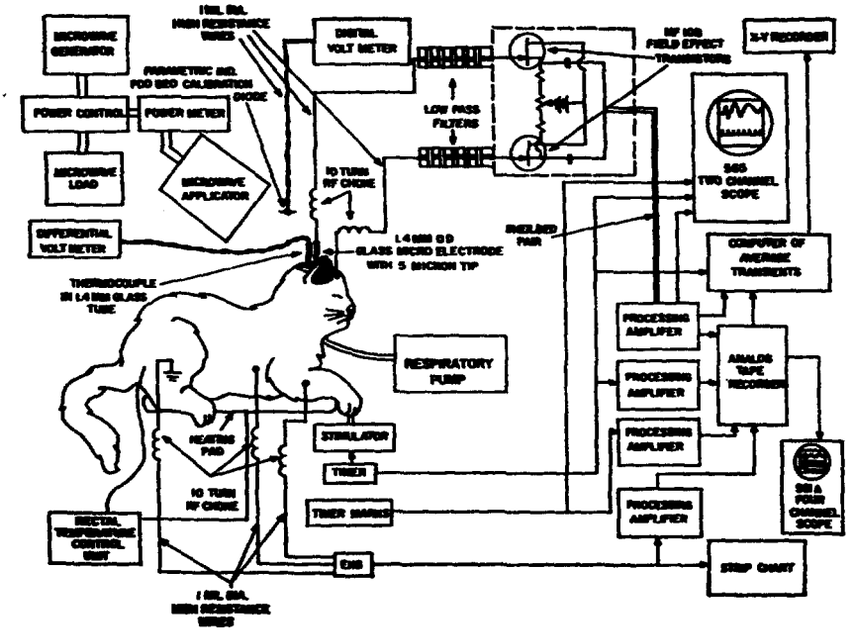

Fig. 16. Block diagram of instrumentation used to quantify CNS effects of microwave radiation in the cat.

TABLE III

CALIBRATION OF 918-MHz MICROWAVE APPLICATOR (8 CM AWAY, 1 W IN) FOR TYPICAL CAT

Region	Absorbed or Incident Power	Method
Free space	2.6 mW/cm² (8 cm *away*) 1.7 mW/cm² (11 cm *away*)	Narda 8110 monitor
In stereotaxic support without cat	2.48 mW/cm²	Narda 8110 monitor
Maximum heating area of thalamus of cat	2.0 mW/cm²	thermographic
Maximum heating area in phantom sphere	1.5 mW/cm² 2.1 mW/cm² 1.4 mW/cm² 0.4 to 0.8	thermographic (8 cm from aperture source) 2.6 mW/cm² (theoretical 1.7 mW/cm² plane wave)
Surface of cat brain	(mW/cm²) 0.54 mW/cm²	microwave diode thermographic
Maximum heating area of thalamus of cat	1.88 mW/cm²	thermocouple (live brain)
Homologous point in opposite thalamus of electrode position	1.23 mW/cm²	thermocouple (live brain)

Fig. 17. Photograph of half-section of cat's head with electrode position shown.

before and after a short-term exposure to high-power microwaves as a function of position in the cat's brain and the changes were converted to absorbed power information.

4) The cat's body was frozen in the stereotaxic support, cast in a Styrofoam block, bisected, returned to room temperature, and rejoined back into the stereotaxic support for a short-term high-intensity exposure. Immediately after the exposure, the thermograph recordings of the induced internal temperature patterns in a half-section of the cat's head were made and converted to power absorption patterns. Typical calibration results are tabulated in Table III.

A photograph of the bisected cat is shown in Fig. 17. Thermograms were taken of the cat's head and also of an equivalent phantom sphere for several different conditions. One set of thermograms was taken without the presence of any recording electrodes, the second set was done with the presence of a saline-filled glass electrode, and the final set was taken with the presence of a standard coaxial metal electrode. No differences were found between the thermograms taken for the first two cases, but a significant change was noted for the metal electrode. Figs. 18 and 19 show the results for the phantom model and cat's head with and without the metal electrodes. The results clearly indicate that a standard metal coaxial electrode normally used for neurophysiological experiments can produce very serious modifications and intensifications of the peak absorbed power density by as much as two orders of magnitude. The widespread use of such electrodes, both in the Soviet Union and in this country, in assessing the biological effects of microwave radiation on the CNS could be resulting in the interpretation of highly localized thermal effects as nonthermal or low-level effects.

The EKG of the cat was recorded and monitored on a strip chart recorder. The EKG was observed to increase with microwave power density and temperature at much higher levels than that required to produce thalamic changes.

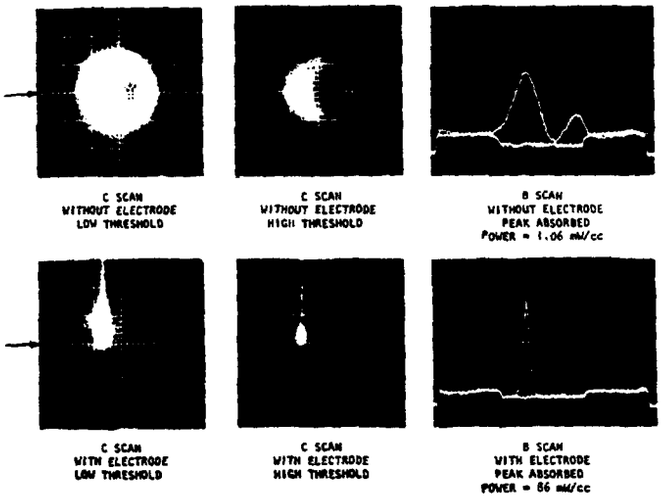

Fig. 18. Thermographic study of effect of coaxial electrode on microwave absorption pattern of spherical phantom of cat brain (6-cm diam). Scale: *C* scans, 1 div = 2 cm; *B* scans, 1 horizontal div = 2 cm, 1 vertical div = 2.5°C. (Incident power density = 2.5 mW/cm².)

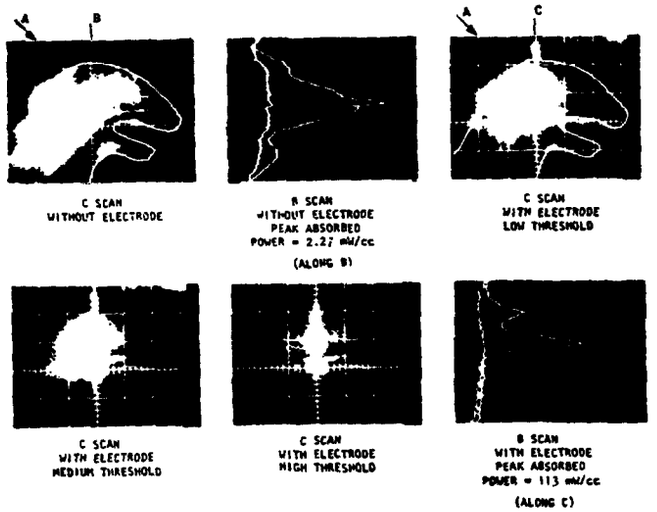

Fig. 19. Thermographic study of effect of coaxial electrode on microwave absorption pattern in brain of cat 49 exposed to 918-MHz aperture source. Scale: *C* scans, 1 div = 2 cm; *B* scans, 1 horizontal div = 2 cm, 1 vertical div = 2.5°C. Subject exposed from top with horizontal *E* vector in plane of paper. (*A* = direction of incident power *B* = vertical center, and *C* = vertical probe line, 1 mm to left of center.) (Incident power density = 2.5 mW/cm².)

The thalamus response characteristics were processed for improved signal-to-noise ratio, both on-line and off-line, by a computer of average transients. The results were plotted by means of an *x–y* recorder with typical results as shown in Fig. 20. Typical thalamus temperature curves are illustrated in Fig. 21, and the measured power absorption patterns are given in Fig. 22. The measurable effects of the microwaves appear to be an induced temperature rise in the thalamus with an associated decrease in latency time of neural responses within the exposed area. Each curve in Fig. 20 is the averaged thalamus response based on 50 stimuli obtained either at the end of each exposure or at the end of each period with no radiation. The peak microwave power absorption density and temperature in the thalamus area are noted on each curve. The latency times between the stimulus and the initial thalamus response (denoted by an upward arrow) and between the initial thalamus response and a distinguishable later event

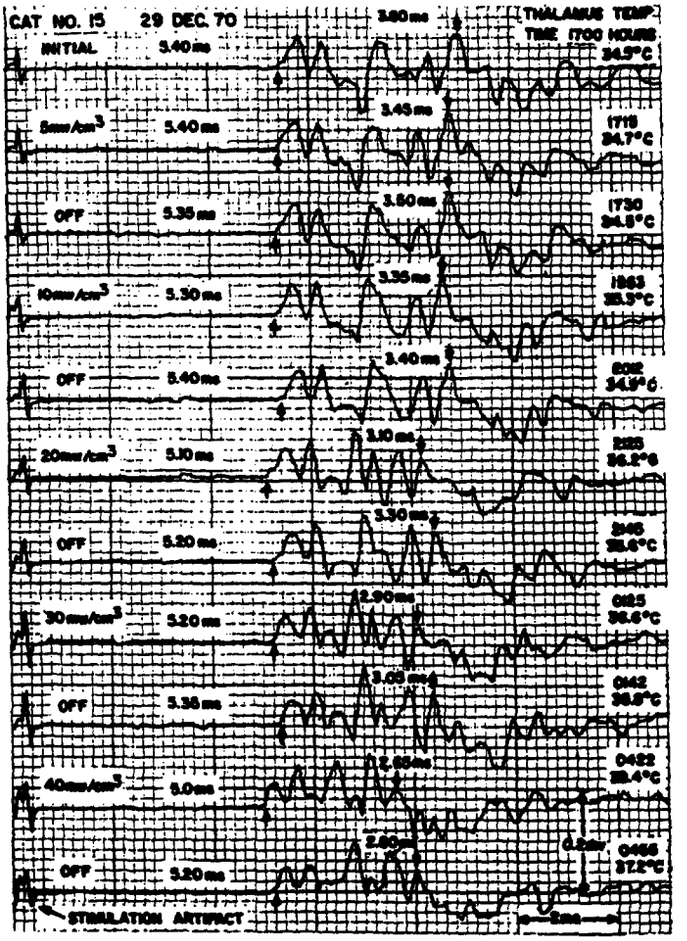

Fig. 20. Effects of microwave radiation on thalamic response of cat to stimulation of contralateral forepaw.

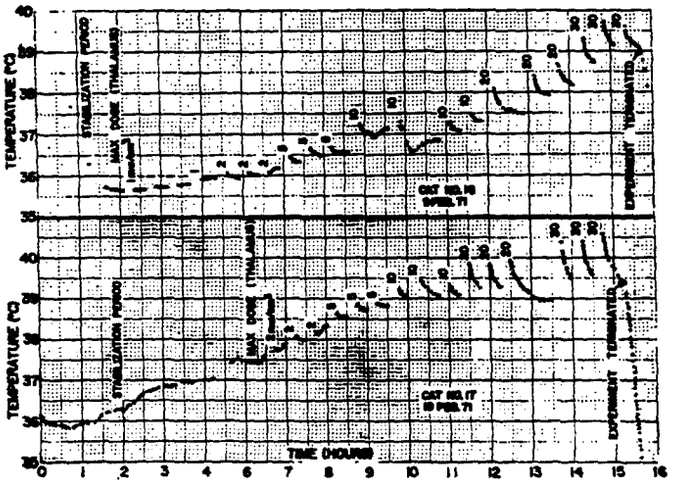

Fig. 21. Thalamus temperature of cats exposed to 918-MHz microwave radiation for 15-min intervals (power off during temperature recordings).

(denoted by a downward arrow) are also noted. The latency between the stimulus artifact and the first arrow represents a neural pathway between the cat's paw and brain, whereas the latency between the arrows is probably more closely associated with pathways within the brain. Experimental results also indicate that both latencies decrease with increasing body temperature of the cat when produced by an increase in temperature of the hot pad, whereas microwaves